IEEE Access
Multidisciplinary | Rapid Review | Open Access Journal

Received 25 March 2024, accepted 2 April 2024, date of publication 5 April 2024, date of current version 17 April 2024.

Digital Object Identifier 10.1109/ACCESS.2024.3385573

RESEARCH ARTICLE

Enhancing Precision in Medical Imaging: A 3D CNN Approach for Fiducial Point Detection in MRI Data

M. V. SUHAS[1], SANJIB SINHA[2,3], N. MARIYAPPA[2,3], H. ANITHA[1], AND KARUNAKAR A. KOTEGAR[1]

[1]Department of Electronics and Communication Engineering, Manipal Institute of Technology, Manipal Academy of Higher Education, Manipal, Karnataka 576104, India
[2]Department of Neurology, National Institute of Mental Health and Neurosciences (NIMHANS), Bengaluru 560029, India
[3]MEG Research Laboratory, National Institute of Mental Health and Neurosciences (NIMHANS), Bengaluru 560029, India

Corresponding authors: N. Mariyappa (mari.thilak@gmail.com) and H. Anitha (anitha.h@manipal.edu)

This work was supported by Indian Council for Medical Research (ICMR) under Grant-in-Aid Scheme of Department of Health Research "Inter-Sectoral Convergence & Coordination for Promotion on Health Research-Approval" under Grant R.11013/23/2021-GIA/HR (Dated 15.11.2021).

ABSTRACT The significance of fiducial marker detection in neuroimaging cannot be overstated, as these markers serve as vital reference points for accurate spatial alignment during image registration. Our proposed model addresses challenges in consistent marker placement and variability during MRI scanning, ensuring reliable localization for subsequent analysis. This paper introduces an innovative approach to fiducial marker detection in T1-weighted MRI volumes, specifically targeting the Left Preauricular Point (LPA), Right Pre-auricular Point (RPA), and Nasion. The implementation employs a 3D Convolutional Neural Network (CNN) to achieve precise localization of these crucial anatomical landmarks. Operating on a high-performance system our algorithm demonstrated exceptional accuracy and sensitivity using MATLAB R2023a as the primary tool for development and evaluation. Rigorous experiments on a diverse dataset showcased the algorithm's robust performance. For RPA detection, the model achieved 96.55% accuracy, emphasizing sensitivity (96.78% recall) and precision (96.35%). LPA detection demonstrated an impressive accuracy of 96.88%, with heightened sensitivity (96.95%) and precision (96.83%). The nasion detection process exhibited precise localization, with a Mean Square Error (MSE) of 0.3439 for 36 volume data. These results highlight the algorithm's potential to enhance accuracy and efficiency in fiducial point detection for improved neuroimaging studies.

INDEX TERMS Fiducial point detection, 3D MRI data, medical imaging, convolutional neural networks.

I. INTRODUCTION

In the dynamic landscape of medical imaging, particularly Magnetic Resonance Imaging (MRI), plays a pivotal role in diagnosing and understanding various neurological conditions [1], [2], [3], [4], [5]. Fiducial markers, such as the Left Pre-auricular Point (LPA), Right Pre-auricular Point (RPA), and Nasion, are critical anatomical landmarks that serve as reference coordinates during image acquisition and subsequent analysis of neuroimaging studies. These fiducial points are used as accurate spatial references facilitating the accurate alignment and orientation of MRI data during image registration with other neuroimaging studies including modalities like electroencephalography (EEG) and magnetoencephalography (MEG) ensuring precision in the localization of brain structures and abnormalities.

The precise identification of fiducial points on three-dimensional (3D) MRI is pivotal for a myriad of applications,

The associate editor coordinating the review of this manuscript and approving it for publication was Kumaradevan Punithakumar.

such as source imaging, anatomical analysis, and surgical planning. However, there are instances where fiducial markers may not be consistently placed on the patient's head during MRI scanning. This variability can arise from factors such as patient positioning, human error, or the absence of standardized procedures. The absence of fiducial points introduces challenges in post-processing tasks, hindering the accuracy of image registration, anatomical localization, and subsequent analysis of brain structures and abnormalities.

Traditionally, the detection of fiducial points has relied on geometric features, machine learning techniques, and image processing algorithms [6]. However, these approaches often encounter challenges in achieving precise detection due to variations in patient anatomy, image artifacts, and modality-specific nuances.

Given that numerous medical conditions manifest in three-dimensional structures, the significance of fiducial points, such as LPA, RPA, and nasion, cannot be overstated in ensuring accurate spatial referencing in medical imaging. These fiducial points represent anatomical structures with specific 3D coordinates. Leveraging 3D Convolutional Neural Networks (CNNs) becomes imperative to realistically capture the intricacies of these structures, particularly in tasks where preserving spatial relationships and positioning is fundamental [7]. Unlike conventional 2D CNNs, which may overlook the three-dimensional context, employing 3D CNNs guarantees a holistic comprehension of the spatial distribution of these anatomical landmarks [8]. Distinct three-dimensional configurations may characterize fiducial points like LPA, RPA, and nasion, and the use of 3D CNNs enhances the extraction of pertinent features associated with these points, facilitating more accurate localization within volumetric data [9]. The adoption of 3D processing minimizes data redundancy, optimizing computational resource utilization, a particularly pertinent efficiency for tasks involving specific point detection in volumetric data.

Our work focuses on the development of a 3D CNN model designed for the precise detection of three specific landmarks: the left auricular point, right auricular point, and nasion in T1-weighted MRI data. The proposed system aims to enhance the reliability and efficiency of neuroimaging studies by ensuring consistent and accurate localization of fiducial points. This work, therefore, not only aims to address the challenges posed by inconsistent fiducial marker placement but also endeavours to significantly contribute to the broader field of neuroimaging. By introducing a state-of-the-art approach to fiducial point detection, we seek to enhance the reliability and efficiency of neuroimaging studies, with the ultimate goal of utilizing these accurately detected fiducial points for MEG-MRI co-registration in future applications.

The subsequent sections of this paper delve into related works, detailing the methodology of the proposed model, evaluating its efficacy, and concluding with insights drawn from our comprehensive study.

II. RELATED WORKS

The exploration of fiducial marker detection within MRI volumes has been an evolving and dynamic field, with researchers employing various methodologies to enhance precision and reliability. This section reviews key works related to fiducial marker detection, underscoring both the advancements and persisting challenges. Research in the literature indicates that manual identification is the common method for pinpointing these anatomical landmarks [11], [12], [13], [14]. The manual identification of these landmarks introduces a subjective error, leading to inaccuracies in MEG-MRI registration.

A. MACHINE LEARNING IN FIDUCIAL MARKER DETECTION

Geometric features, machine learning techniques, and image processing algorithms have been pivotal in fiducial marker detection [6]. Chen et al. [15] focus on extracting distinctive features from MR images to identify fiducial points, employing both geometric features extraction and intensity-based information. Amoroso et al. [16] incorporate a method that integrates image segmentation, feature extraction, and pattern recognition. Pereira et al. [17] utilize salient features and discrete deformable models, combining feature extraction, model fitting, and optimization techniques for automatic landmark detection. Billot et al. [18] address challenges in detecting and tracking landmarks in dynamic MRI time-series data, employing temporal analysis, feature tracking, or dynamic modeling. Additionally, Chang et al. [19] employ automated techniques, utilizing machine learning or pattern recognition for improved accuracy in landmark detection.

These approaches have demonstrated efficacy but are not without limitations. Variations in patient anatomy, image artifacts, challenges in handling complex deformations and modality-specific nuances, computational complexity often pose challenges, leading to suboptimal detection accuracy.

Lin et al. [20] present a comprehensive approach for aligning MEG, MRI, and DIG data using the 3D Generalized Hough Transform (GHT). Three algorithms facilitate MEG-DIG and MRI-DIG co-registration, employing DIG markers and HPI positions. The 3D GHT detects and matches anatomical landmarks between modalities, enhancing co-registration accuracy and automation.

Prabhu et al. [21] propose an automated method for LPA, RPA, and nasion detection in MR images without fiducial markers. Their Region-Based Convolutional Neural Network (R-CNN) model identifies the Temporomandibular Joint (TMJ) relative to LPA and RPA, while image processing locates nasion. The handcrafted R-CNN achieves successful TMJ detection, with a registration error of 3.6028 ± 1.4037, 4.0512 ± 1.736, and 2.7118 ± 2.7942 mm for LPA, RPA, and nasion in automated MEG-MRI registration compared to manual registration. This study underscores the efficacy of

deep learning and image processing for marker-less anatomical landmark detection, improving MEG-MRI alignment.

Zheng et al. [22] propose an AI-based pipeline for automated epileptic source detection from MEG. Their method achieves MEG-MRI co-registration without manual intervention, utilizing an autolabeling technique and a pattern recognition approach. This process automates fiducial point calibration, including nasion, LPA, and RPA, through an image-feature-based landmark labeling algorithm and iterations of the iterative closest point algorithm. The method relies on features extracted from individual anatomical images.

B. GAPS AND OPPORTUNITIES

While existing literature has made significant strides in fiducial marker detection, there remains a gap in achieving consistent and accurate localization, particularly in the context of 3D MRI volumes. This motivates our work, which introduces a dedicated 3D CNN model tailored for the precise detection of specific fiducial points in T1-weighted MRI data.

By synthesizing insights from traditional methods, recent machine learning approaches, and the emerging realm of 3D imaging, our proposed model seeks to address the limitations identified in current literature, paving the way for improved accuracy and reliability in fiducial marker detection for neuroimaging studies. The following section outlines the methodology employed in developing our novel 3D CNN model for fiducial point detection.

III. METHODOLOGY

The precise detection of fiducial points in T1-weighted MRI scans is achieved through careful preprocessing, the design of an appropriate network architecture, and the implementation of effective training procedures. The step-by-step methodology employed for this purpose is described in this section.

A comprehensive approach was utilized for anatomical landmark detection in medical imaging. The LPA and RPA were identified through a 3D CNN, and advanced image processing techniques were employed to localize the nasion. The necessity for this hybrid approach arose from the limitations of relying solely on a 3D CNN. Importantly, defaced images are commonly found in publicly available MRI volume datasets, and crucially, the section containing the nasion is often absent from these datasets. Therefore, the incorporation of advanced image processing methods was deemed essential to address these challenges and accomplish accurate nasion localization.

The algorithm was implemented on a high-performance system featuring a 12th Gen Intel Core i9- processor, 128 GB RAM, and an NVIDIA RTX A5000 GPU. MATLAB R2023a served as the primary tool for implementing and evaluating the algorithm, ensuring a comprehensive and effective approach to fiducial point detection.

A. DETECTION OF LPA AND RPA

1) DATASET AND PREPROCESSING

The dataset for training the CNN model was gathered from three distinct MRI datasets on OpenNeuro database [23], [24], [25], each originating from different sources and clinical contexts. By merging these datasets, we created a single, comprehensive 3D CNN training dataset. The resulting dataset contains 500 head MRI scans, providing a rich and diverse set of images for training and evaluation. One benefit of utilizing the dataset from OpenNeuro is that the head MRIs come pre-labelled with fiducial markers. This eliminates the laborious process of manually labeling, a crucial step in training and validating neural networks. The model was also validated on the dataset obtained from MEG Research Centre at NIMHANS, Bangalore, India with IEC approval(NIMH/DO/IEC(BS&NS DIV.)10th MEETING/2018).

The T1-weighted MRI datasets from the OpenNeuro database underwent comprehensive preprocessing steps. These steps included normalization to a standardized intensity range, elimination of noise through thresholding, and hole filling using morphological operations. These preprocessing stages aimed to ensure consistency in image intensity and resolution, facilitating effective feature learning by the network.

Following the preprocessing phase, we obtained 2 classes of training patches measuring 30×50x50 from the entire set of 500 3D MRI datasets for training the 3D CNN. The positive class patches were extracted with manually labelled LPA and RPA coordinates available with the dataset serving as the centroid. Data augmentation techniques, such as rotation around the centroid, scaling, and random cropping, were implemented to enhance dataset diversity, generating a total of 116 patches per auricular point. The data resulting from these operations were assigned the label 1 representing the positive class.

Additionally, patches representing the negative class were generated by shifting across different axes away from the LPA/RPA fiducial points. Employing nested loops, with an initial minimum shift of 5 pixels in the x, y, and z directions, while keeping two directions constant at a time, the centroid was shifted away from the LPA/RPA points. These negative patches partially overlapped with each other and the positive patch. This process resulted in a total of 116 patches (around LPA/RPA) per auricular point, labelled distinctly as class 2. The number of negative patches (58,000) equalled that of the positive class after augmentation, contributing to a total of 116,000 patches per auricular point across the entire 500 dataset.

2) NETWORK ARCHITECTURE

The classification of extracted patches into positive and negative classes is performed by the network architecture depicted in Figure 2 comprising a 3D CNN. The input layer accepts the 3D patches of dimension [$30 \times 50 \times 50$].

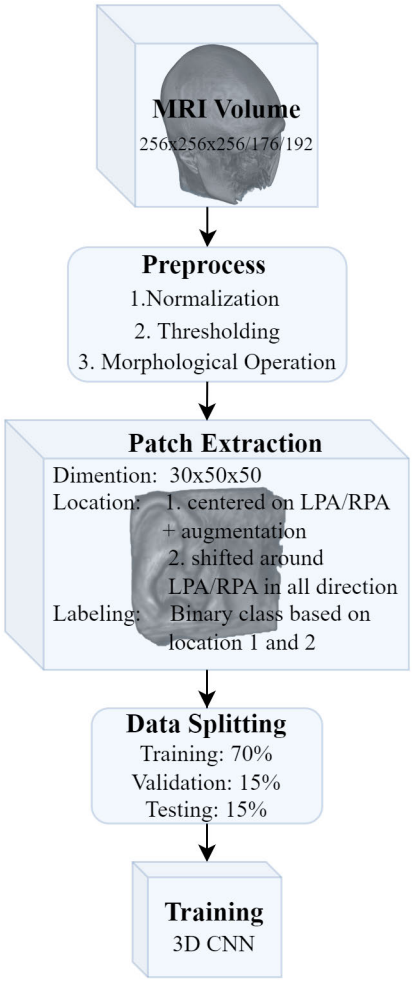

FIGURE 1. Processflow of LPA/RPA patch extraction and training.

The network consists of three convolutional blocks, each containing a 3D convolutional layer, batch normalization, and ReLU activation. Two max-pooling layers with a pool size of 2 and a stride of 2 follow the first and second convolutional blocks. The architecture also includes a fully connected layer with 256 neurons, followed by batch normalization, ReLU activation, and a dropout layer with a rate of 0.5. The output layer consists of a fully connected layer with 2 neurons, a softmax layer for probability distribution, and a classification layer.

3) TRAINING PROCEDURE

The extracted patch dataset is divided into training, validation, and test sets to assess model performance. A typical split of 70% for training, 15% for validation, and 15% for testing was involved. The CNN model is trained using the training dataset to learn the prediction of patches by minimizing the defined loss function. The trained model is evaluated on the test set to assess its generalization capability and performance in detecting the patches.

We conducted a grid search over various combinations of hyperparameters to optimize the performance of the CNN model. Table 1 lists the various hyperparameters and the corresponding tested values.

TABLE 1. Hyperparameter grid search details.

Hyperparameter	Values Tested
Learning Rates	0.001, 0.01, 0.1
Batch Sizes	64, 128, 256
Optimization Algorithms	Adam [26] , RMSprop [27], SGD [28]
Learning Rate (LR) Schedules	Exponential Decay, Cosine Annealing, Cyclic LR, Piecewise LR
Number of Epochs	10, 20, 30

These combinations aimed to find the optimal configuration that maximized the performance of the CNN model on the task of fiducial point detection in neuroimaging data. The best model identified through grid search involved the Adam optimizer with an initial learning rate of 0.01, a batch size of 128, and a piecewise learning rate schedule that reduced the learning rate by a factor of 0.1 every 5 epochs, and training for 20 epochs utilizing GPU acceleration. Adam optimizer maintains moving averages for each parameter, adapting learning rates dynamically during training. This adaptive approach is effective for handling sparse gradients, noisy data, and non-stationary objectives, providing a balance between quick convergence and stability during training. Training progress, including metrics like loss and accuracy is visually observed.

The model's performance was monitored on the validation set to prevent overfitting. Validation was performed every 50 iterations using a separate dataset, ensuring the model's generalization ability was assessed. Early stopping was applied when the validation loss plateaus, with a patience of 10 validations without improvement, ensuring efficient model convergence.

4) LPA AND RPA DETECTION

Two separate model were trained for LPA and RPA, hence, the detection of LPA and RPA is conducted independently. The MRI volume is loaded and subjected to preprocessing using the same procedures employed in the training phase to ensure consistency.

Patches of dimensions $30 \times 50 \times 50$ are systematically extracted from predefined regions of interest and input into the pre-trained CNN for predictive analysis. Specific regions of interest within the preprocessed MRI volume are delineated for focused examination, with patches sourced from the left side of the head for LPA detection and the right side for RPA detection. This targeted approach not only streamlines computational demands but also reduces processing time. The identified point with the highest confidence is selected, and its center point represents the coordinates of either LPA or RPA.

B. DETECTION OF NASION

The nasion is often a landmark on the mid-sagittal slice of the head. To locate the nasion on a mid-sagittal slice, we would

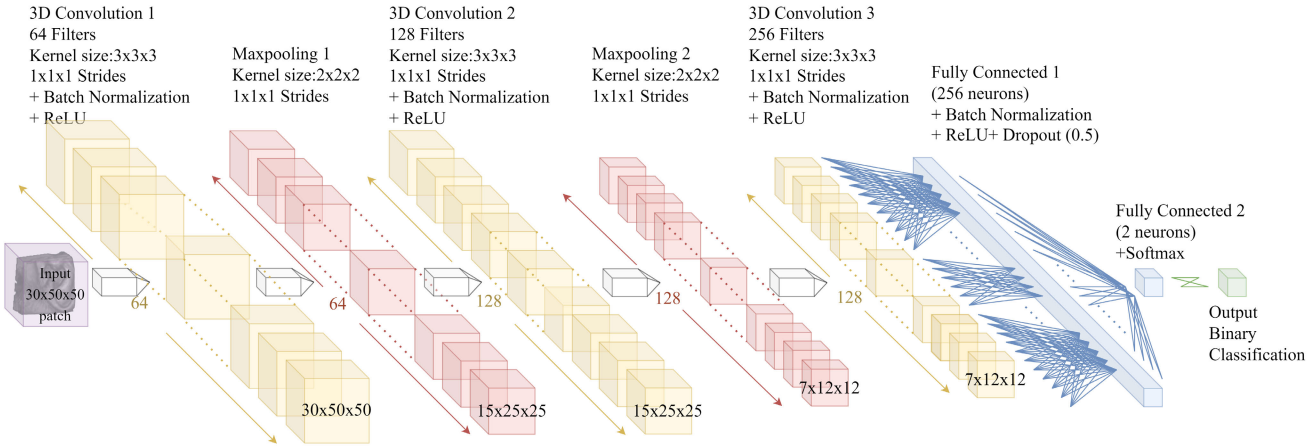

FIGURE 2. Overview of 3D CNN architecture implemented in Matlab®.

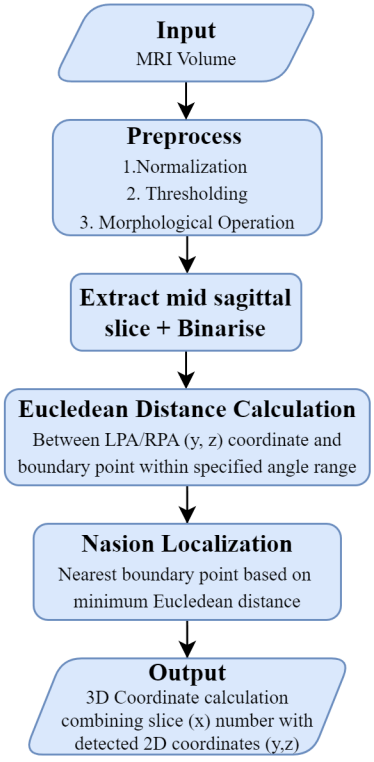

FIGURE 3. Process flow of nasion coordinate detection.

look for the point where the frontal bone and the nasal bones come together [29], typically appearing as a depression or a distinct landmark on the image. The steps involved in the detection of nasion coordinates are explained below and depicted in Fig. 3.

Once the preprocessing was completed, the nasion detection process involved the selection of the mid-sagittal slice (since nasion lies on this plane), which was then converted into a binary image. Within this binary representation, boundary points, where the pixel value changes from 1 to 0,

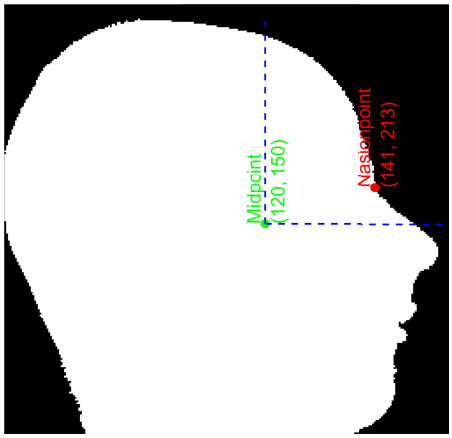

FIGURE 4. The preprocessed mid-sagittal slice depicting the midpoint selected from the LPA and RPA reference and the range restriction lines (blue dashed line) within which the nearest boundary is searched for nasion coordinates.

were identified, representing the edges or contours of anatomical structures present in the image, specifically the edge of the entire head as shown in Fig. 4.

The subsequent step involved calculating Euclidean distances from the mid-point coordinate (derived from the previously detected LPA and RPA coordinates) to the boundary within the angle that encompasses the nasion point and the limited surrounding region (at a right angle from the mid-point towards the fronto upper face region) as marked by the blue dashed line on Fig. 4. This targeted angle ensured avoiding the false negative detection of nasion coordinates.

The final determination of the nasion's precise location was made by selecting the closest boundary point based on the minimum Euclidean distance within the designated angle range. While the mid-sagittal slice number gives the x coordinate, the detected 2-D coordinates provide the (y, z) coordinates, which are combined to obtain the 3D coordinate of the nasion point.

This selection process ensures that the detected nasion point aligns accurately with the expected anatomical features, enhancing the reliability of nasion detection. This multi-step approach, from preprocessing to angle-based selection, ensured the accurate and reliable detection of nasion in MRI data, addressing the complexities of 3D spatial relationships and enhancing the overall efficacy of fiducial point detection.

C. EVALUATION METRICS

To quantitatively assess the model's performance in detecting the LPA and RPA, we employed various evaluation metrics, including:

Accuracy: The percentage of correct landmark predictions out of the total predictions.

$$Accuracy = \frac{TP + TN}{TP + TN + FP + FN} \tag{1}$$

Recall (Sensitivity): The ratio of true positive predictions to the total actual left auricular points.

$$Recall = \frac{TP}{TP + FN} \tag{2}$$

Specificity: The ratio of true negatives to the total negatives, providing an indicator of the model's ability to correctly identify non-landmark areas.

$$Specificity = \frac{TN}{FP + TN} \tag{3}$$

Precision: The ratio of true positives to the total positive predictions, measuring the model's accuracy in landmark localization.

$$Precision = \frac{TP}{TP + FP} \tag{4}$$

F1 Score: The harmonic mean of precision and recall, providing an overall measure of the model's performance.

$$F1 = \frac{2 * Precision * Recall}{Precision + Recall} \tag{5}$$

In the above equations, TP, TN, FP, FN are True Positive, True Negative, False Positive and False Negative respectively.

Following detection of LPA, RPA and nasion, Euclidean distance (ED) (Eq. 3) between the detected point and the ground truth was computed.

$$\text{ED} = \sqrt{(x_T - x_D)^2 + (y_T - y_D)^2 + (z_T - z_D)^2} \tag{6}$$

where x_D, y_D, z_D are the detected coordinates and x_T, y_T, z_T are the ground truth coordinates.

To quantify the overall accuracy, Mean Squared Error (MSE) (Eq. 7) is computed which is a measure of average squared difference between corresponding values in detected and ground truth value.

$$MSE = \frac{1}{n}\sum_{i=1}^{n}(x_T - x_D)_i^2 + (y_T - y_D)_i^2 + (z_T - z_D)_i^2 \tag{7}$$

where x_D, y_D, z_D are the detected coordinates and x_T, y_T, z_T are the ground truth coordinates.

TABLE 2. Performance metrics of LPA and RPA patch detection.

Metrics in percentage	RPA	LPA
Accuracy	96.55	96.88
Recall	96.78	96.95
Specificity	97.00	97.17
Precision	96.35	96.83
Average F1 Score	96.67	97.00

By assessing the model's performance using these metrics, we gain a comprehensive understanding of its accuracy and reliability in detecting the fiducial points point in T1-weighted MRI scans. The subsequent section focuses on the evaluation of the proposed model's efficacy.

IV. EXPERIMENTS AND RESULTS

Given that the identification of LPA and RPA, as well as the determination of nasion, involved distinct procedures, the results are presented in separate sections for clarity. This approach facilitates a comprehensive examination of each detection process, ensuring a detailed analysis of the outcomes for LPA, RPA, and nasion.

A. RESULTS OF 3D CNN TRAINING AND LPA AND RPA DETECTION

We conducted experiments using 3D CNN architectures to detect the LPA, RPA in MRI scans. The results demonstrate superior performance of integrated dataset for landmark detection, with precise localization of these anatomical points.

Training was conducted separately for the LPA and RPA patches datasets, utilizing 70% of the data to generate two distinct CNN models. Validation occurred concurrently during training, involving 15% of the dataset. The training progress for RPA dataset is illustrated in Fig. 5. At the conclusion of the 5th epoch out of the set 10 epochs (due to early stop criterion with a patience of 10), a validation accuracy of 96.16% was achieved. The entire training procedure was completed within 37 minutes. A similar setup for LPA dataset yielded a validation accuracy of 97.18%. The loss curve consistently followed the anticipated declining trend throughout the training process as could be seen in the Fig. 5.

The evaluation of the algorithm's efficacy took place on a distinct 15% test dataset dedicated to RPA and LPA detection. The outcomes of this evaluation are encapsulated in Table 2. The confusion matrices corresponding to these detections are illustrated in Figures 6 and 7.

For LPA detection, the algorithm performed impressively with an overall accuracy of 96.88%. The model achieved a 96.95% recall, indicating heightened sensitivity to true positives, and a specificity of 97.17% for correctly identifying true negative cases. Precision for LPA was 96.83%, demonstrating the model's reliability in minimizing false positives. The average F1 score for LPA detection was 97%, confirming robust performance.

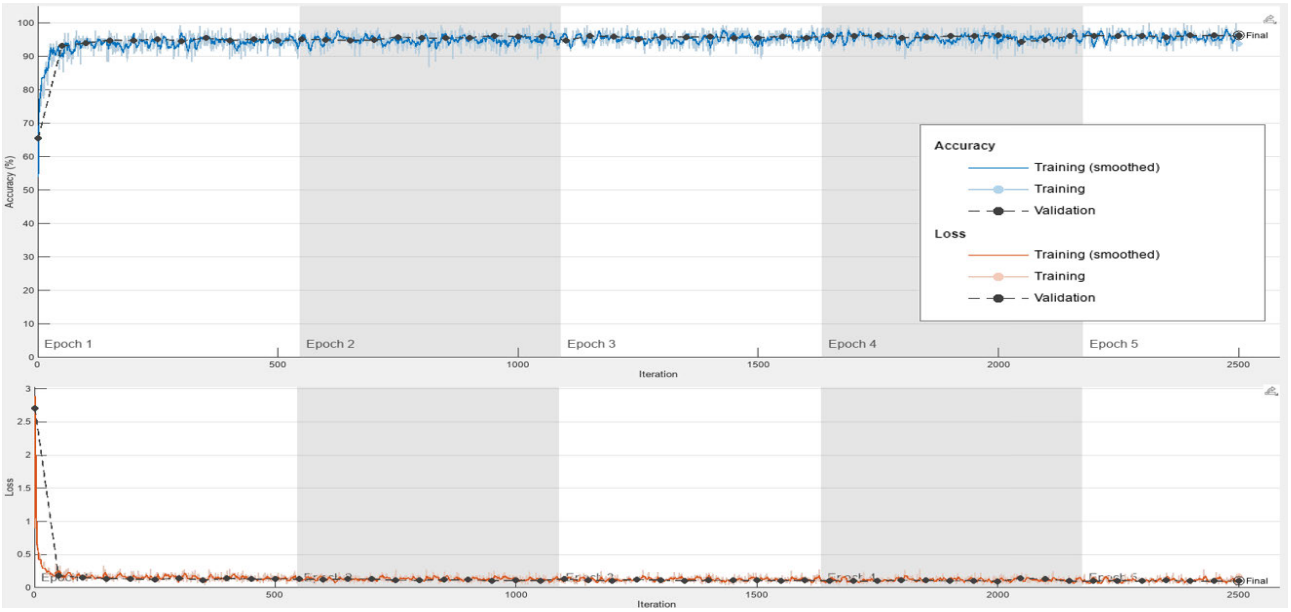

FIGURE 5. The plot illustrating the training accuracy and loss for the RPA dataset depicts a continual rise in training accuracy, culminating in a final accuracy of 96.16%, accompanied by a concurrent decrease in loss.

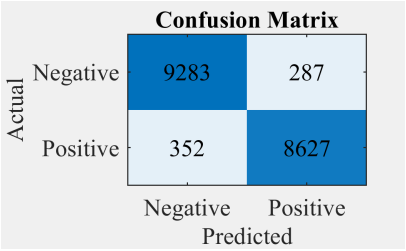

FIGURE 6. Confusion matrix for RPA detection.

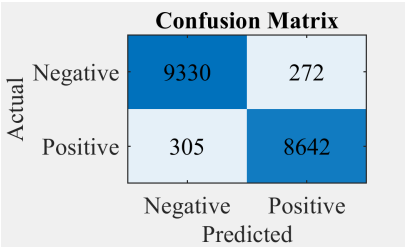

FIGURE 7. Confusion matrix for LPA detection.

The algorithm demonstrated strong performance for the RPA, achieving 96.55% accuracy, with a notable 96.78% recall, emphasizing its sensitivity to true positives. The model also showed high specificity at 97%, minimizing false positives, and precision at 96.35%, ensuring confident identification. The average F1 score of 96.67% provided a comprehensive assessment of overall effectiveness.

The evaluation of the LPA and RPA detection algorithm is based on a comprehensive dataset consisting of 36 3D MRIs. As reflected by the examples, on the first 5 rows of Table 3 for LPA and next 5 rows of Table 3 for RPA, the collective analysis suggests an overall reasonable performance of the algorithm in accurately identifying the preauricular points across various instances. The smaller Euclidean distances observed in numerous entries indicate successful alignment between the detected coordinates and the ground truth values. This alignment underscores the algorithm's capacity to provide precise localization in a significant portion of the dataset. However, the presence of larger distances in instances like and suggests variability and challenges in certain detection scenarios.

TABLE 3. Sample list of detected and actual fiducial point coordinates along with individual Euclidean Distance (ED in mm).

Fiducial	Detected	Ground truth	ED in mm
LPA	[9,110,121]	[10,111,123]	2.4494
	[22,132,104]	[25,132,107]	4.2426
	[20,127,104]	[20,126,105]	1.4142
	[19,126,109]	[21,127,112]	3.7416
	[6,117,113]	[5,116,112]	1.7320
RPA	[163,118,118]	[165,119,118]	2.2360
	[173,112,127]	[172,111,128]	1.7320
	[170,120,111]	[169,119,111]	1.4142
	[163,113,123]	[160,114,122]	3.3166
	[176,124,107]	[175,122,107]	2.2360
	[207,116,74]	[203,115,72]	4.5825
Nasion	[104,226, 144]	[103, 225, 142]	2.4494
	[90, 261, 172]	[90, 261, 172]	0.0000
	[80, 226, 140]	[79, 226, 141]	1.4142
	[96, 217, 142]	[95, 217, 142]	1.0000
	[72, 222, 138]	[72, 222, 138]	0.0000

B. RESULTS OF NASION DETECTION

While the approach for nasion coordinate detection was using image processing and not 3D CNN, We quantitatively evaluated the performance of the method using Euclidean

TABLE 4. Overall evaluation metrics calculated between proposed and manual method for 36 datasets.

Metrics (in mm)	LPA	RPA	NASION
Mean ED	2.8852	2.8245	0.9025
Standard Deviation of ED	1.1113	1.0113	1.0359
Mean Square Error	2.875	2.9885	0.3439
Standard Deviation of Squared Error	3.1550	4.6476	2.9619

distance and mean square error. The last 5 rows of Table 3 presents examples of the comparison between detected and ground truth 3D coordinates of the nasion on 3D MRI volume, with corresponding Euclidean distances. The majority of the results exhibit precise detection, with zero Euclidean distances indicating a close alignment between detected and ground truth coordinates. Small deviations, observed in certain coordinates, result in reasonable distances. While some cases reveal systematic errors and outliers, the majority of the detections align closely with the ground truth. This suggests that the algorithm generally performs well in accurately identifying the nasion's 3D coordinates in the MRI volume. Consideration of specific outliers and systematic errors could further enhance the algorithm's performance for this specific localization task.

C. ANALYSIS OF OVERALL PERFORMANCE METRICS

It is important to note that the table 3 provides only a partial view of the algorithm's overall performance, as it encompasses a subset of possibilities. The detection process extends beyond the shown instances, and a comprehensive evaluation involves considering the algorithm's behavior across the larger dataset for validation consisting of 36 MRi volumes using the metrics such as Mean ED, Standard Deviation of ED, MSE and Standard Deviation of Squared Error which is shown in table 4.

The Mean ED for LPA and RPA suggests that these auricular points are detected with slightly higher average distance from the ground truth compared to nasion. This indicates a potential challenge in accurately locating auricular points. The smaller standard deviations for RPA and nasion compared to LPA suggest that detections for RPA and nasion are more consistent across different datasets. MSE of LPA and RPA indicates a moderate level of error across the dataset. While the algorithm shows promise, addressing instances of deviation and outliers could enhance its precision for improved performance in diverse scenarios. The lower MSE for nasion indicates that the algorithm for nasion detection performs more accurately with smaller squared differences between detected and ground truth points. The higher standard deviations for LPA and RPA compared to nasion suggest that there is more variability in the squared errors for auricular points across different datasets.

D. 3D VISUALIZATION OF THE FIDUCIAL POINTS

After successfully identifying the coordinates of the LPA, RPA, and nasion, the next step involves visualizing these coordinates within the 3D MRI volume. This visualization process is exemplified in Figure 8, where the detected coordinates are represented by distinct green dots, while the actual coordinates are denoted by red dots. Additionally, the coordinate values, both actual and detected, are concurrently presented in the command window.

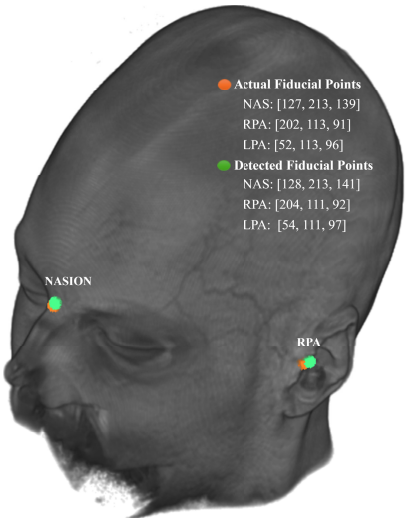

FIGURE 8. 3D Visualization of the fiducial points.

The integration of visual representation in Figure 8, along with simultaneous display of coordinate values in the command window, provides a comprehensive and accessible means to evaluate the performance of the coordinate detection process in relation to the actual anatomical landmarks. The graphical representation provides a qualitative insight into the accuracy of the coordinate detection process and facilitates a direct comparison between the detected and actual positions of these fiducial points. By employing red and green dots for the actual and detected coordinates, respectively, the visual contrast enhances the observer's ability to discern any disparities or alignments. The quantitative display, enables a detailed examination of the numerical data associated with the fiducial points serving to aid further analysis and validation of the accuracy of the coordinate detection algorithm.

V. COMPARATIVE ANALYSIS OF AUTOMATED TECHNIQUES FOR FIDUCIAL MARKER DETECTION/MEG-MRI CO-REGISTRATION

The accurate localization of fiducial markers for the precise alignment of different imaging modalities, are crucial for effective clinical analysis and treatment planning. This section presents a comparative analysis of automated techniques for fiducial marker detection and MEG-MRI co-registration, focusing on four methodologies. Table 5 provides a detailed comparison of these automated techniques, highlighting their objectives, methodologies, and performance metrics.

TABLE 5. Comparison between automated techniques for fiducial marker detection/MEG-MRI Co-registration.

Approach	3D GHT Co-Registration [20]	R-CNN Approach [21]	AMSI Pipeline [22]	Proposed Method
Objective	Automated co-registration of MEG and MRI data	Automated detection of anatomical landmarks for MEG-MRI registration	Automated detection and localization of epileptic sources from MEG data	Automated detection of fiducial points (anatomical landmarks) in MRI data
Methodology	3D Generalized Hough Transform	R-CNN for detecting TMJ and image processing for nasion detection	AI-based pipeline combining autolabeling, CNNs, and clustering	3D CNN for localization of LPA, RPA, and image processing for nasion detection
Performance Metrics	3 subjects average RMS error for MEG–MRI data (Mean: 2.88 mm, Maximum: 5.63 mm, Minimum: 1.24 mm)	Comparison between manual and automated marking for 42 patients (mean $\pm$ standard deviation in mm: LPA: 3.6028 $\pm$ 1.4037, RPA: 4.0512 $\pm$ 1.736, Nasion: 2.7118 $\pm$ 2.7942)	48 patient median MEG-MRI coregistration error (AMSI:2.34 mm vs. Manual:3.76 mm)	Comparison between manual and automated marking for 36 patients (mean $\pm$ standard deviation in mm: LPA: 2.8852 $\pm$ 1.1113, RPA: 2.8245 $\pm$ 1.0113, Nasion: 0.9025 $\pm$ 1.0359)

The 3D GHT Co-Registration method, proposed by Lin et al. [20], focuses on automating the co-registration process of MEG and MRI data. This technique leverages the 3D GHT to achieve accurate alignment between different imaging modalities. The method demonstrates promising results with an average RMS error of 2.88 mm for MEG-MRI data, indicating reliable co-registration performance.

Prabhu et al. [21] introduced the R-CNN approach for automated detection of anatomical landmarks for MEG-MRI registration. By employing R-CNN for landmark detection and image processing techniques for nasion detection, this method enhances accuracy and reliability in medical image registration. However, the study reports mean errors ranging from 3.6028 $\pm$ 1.4037 mm to 4.0512 $\pm$ 1.736 mm, suggesting potential challenges in precise landmark localization.

The Automated Magnetic Source Imaging (AMSI) Pipeline, proposed by Zheng et al. [22], offers an AI-based solution for detecting and localizing epileptic sources from MEG data. By combining autolabeling, CNNs, and clustering techniques, the AMSI Pipeline achieves efficient and objective analysis of MEG data. The results demonstrate a significant improvement in coregistration accuracy compared to manual methods, with a median error of 2.34 mm.

Our proposed method with an image processing and 3D CNN approach achieves precise automatic localization of anatomical landmarks, including the LPA, RPA, and nasion, in MRI data enhancing the accuracy and efficiency of fiducial marker detection. Our results indicate mean square errors ranging from 2.8245 $\pm$ 1.0113 mm to 2.8852 $\pm$ 1.1113 mm,for RPA and LPA with a mean square error of 0.9025 $\pm$ 1.0359 for nasion detection.

In summary, each automated technique offers distinct advantages in improving medical imaging analysis and diagnosis. While the 3D GHT Co-Registration method excels in accurate alignment of imaging modalities, the R-CNN Approach and AMSI Pipeline demonstrate efficiency and objectivity in anatomical landmark detection and epileptic source localization, respectively. Our proposed method contributes to the field by providing a reliable and efficient solution for fiducial marker detection in MRI data, facilitating enhanced MEG-MRI co-registration and subsequent medical image analysis.

VI. CONCLUSION

In this paper, we have presented an approach of image processing and 3D CNN models trained with enhanced dataset in brain imaging, with a specific focus on landmark detection. The integration of three T1-weighted MRI datasets from the OpenNeuro database resulted in a comprehensive dataset of 500 head MRI scans, enhancing the precision of anatomical landmark detection. Our approach significantly improves the accuracy and robustness of landmark detection, offering potential benefits for neuroanatomical research, clinical practice, and surgical planning.

In the context of nasion detection using image processing, while the squared differences between detected and ground truth coordinates are relatively small, a detailed examination of instances with larger Euclidean distances and outliers in the complete dataset could guide refinements to fine-tune the algorithm and address potential limitations.

The 3D CNN approach demonstrates promising accuracy during LPA and RPA detection, with instances showing close alignment to ground truth coordinates, as evidenced by smaller Euclidean distances. However, variations and outliers contribute to a moderate MSE. While the algorithm accurately captures fiducial points in certain cases, there is room for improvement to address systematic errors and enhance overall precision. The MSE value serves as a valuable quantitative metric for guiding further refinements, ensuring the algorithm's robustness in real-world scenarios.

The analysis of overall performance metrics highlights differences in the performance of algorithms for detecting LPA, RPA, and nasion on MRI volumes. While the algorithms for auricular points exhibit higher mean distances, larger standard deviations, and higher mean squared errors, the algorithm for nasion detection demonstrates better accuracy, consistency, and lower errors.

In summary, while the algorithm exhibits acceptable performance, ongoing optimization efforts can refine its accuracy and reliability for auricular point detection. Overall, our contributions provide a valuable step forward in advancing fiducial marker detection for neuroimaging studies, offering a promising avenue for improving accuracy and efficiency in medical image analysis and clinical applications.

ACKNOWLEDGMENT

The dataset for validation was provided by MEG Research Centre, Department of Neurology, National Institute of Mental Health and Neuro Sciences (NIMHANS), Bengaluru, India, with IEC Approval [NIMH/DO/IEC (BS&NS DIV.) 10th MEETING/2018].

REFERENCES

[1] M. Živanović, A. A. Trenkić, V. Milošević, D. Stojanov, M. Mišić, M. Radovanović, and V. Radovanović, "The role of magnetic resonance imaging in the diagnosis and prognosis of dementia," *Bosnian J. Basic Med. Sci.*, vol. 30, pp. 209–224, Nov. 2022, doi: 10.17305/bjbms.2022.8085.

[2] A. M. Al-Radaideh and E. M. Rababah, "The role of magnetic resonance imaging in the diagnosis of Parkinson's disease: A review," *Clin. Imag.*, vol. 40, no. 5, pp. 987–996, Sep. 2016, doi: 10.1016/j.clinimag.2016.05.006.

[3] S. Debette, S. Schilling, M.-G. Duperron, S. C. Larsson, and H. S. Markus, "Clinical significance of magnetic resonance imaging markers of vascular brain injury: A systematic review and meta-analysis," *JAMA Neurol.*, vol. 76, no. 1, p. 81, Jan. 2019, doi: 10.1001/jamaneurol.2018.3122.

[4] C. Granziera, "Quantitative magnetic resonance imaging towards clinical application in multiple sclerosis," *Brain*, vol. 144, no. 5, pp. 1296–1311, May 2021, doi: 10.1093/brain/awab029.

[5] D. Pan, A. Zeng, L. Jia, Y. Huang, T. Frizzell, and X. Song, "Early detection of Alzheimer's disease using magnetic resonance imaging: A novel approach combining convolutional neural networks and ensemble learning," *Frontiers Neurosci.*, vol. 14, May 2020, Art. no. 501050, doi: 10.3389/fnins.2020.00259.

[6] G. Wang, W. Li, and S. Ourselin, "Automatic brain tumor segmentation based on cascaded anisotropic convolutional neural networks," in *Proc. Int. Conf. Med. Image Comput. Comput.-Assist. Intervent (MICCAI)*, 2016, pp. 178–186.

[7] E. Gibson, W. Li, C. Sudre, L. Fidon, D. I. Shakir, G. Wang, Z. Eaton-Rosen, R. Gray, T. Doel, Y. Hu, T. Whyntie, P. Nachev, M. Modat, D. C. Barratt, S. Ourselin, M. J. Cardoso, and T. Vercauteren, "NiftyNet: A deep-learning platform for medical imaging," *Comput. Methods Programs Biomed.*, vol. 158, pp. 113–122, May 2018.

[8] W. Bai et al., "Automated cardiovascular magnetic resonance image analysis with fully convolutional networks," *J. Cardiovascular Magn. Reson.*, vol. 20, no. 1, p. 65, Feb. 2018.

[9] M. Drozdzal, "The importance of skip connections in biomedical image segmentation," *Proc. Int. Workshop Deep Learn. Med. Image Anal. Int. Workshop Large-Scale Annotation Biomed. Data Expert Label Synth.*, pp. 179–187, 2016.

[10] M. H. Hesamian, W. Jia, X. He, and P. Kennedy, "Deep learning techniques for medical image segmentation: Achievements and challenges," *J. Digit. Imag.*, vol. 32, no. 4, pp. 582–596, Aug. 2019.

[11] S. S. Dalal, S. Rampp, F. Willomitzer, and S. Ettl, "Consequences of EEG electrode position error on ultimate beamformer source reconstruction performance," *Frontiers Neurosci.*, vol. 8, p. 42, Mar. 2014.

[12] L. Troebinger, J. D. López, A. Lutti, S. Bestmann, and G. Barnes, "Discrimination of cortical laminae using MEG," *NeuroImage*, vol. 102, pp. 885–893, Nov. 2014.

[13] C. Whalen, E. L. Maclin, M. Fabiani, and G. Gratton, "Validation of a method for coregistering scalp recording locations with 3D structural MR images," *Hum. Brain Mapping*, vol. 29, no. 11, pp. 1288–1301, Nov. 2008.

[14] A. Hillebrand, "The use of anatomical constraints with MEG beamformers," *NeuroImage*, vol. 20, no. 4, pp. 2302–2313, Dec. 2003.

[15] X. Chen, J. J. Corso, L. Lu, and D. N. Metaxas, "Automatic identification of fiducial points for image registration in magnetic resonance images," in *Proc. Int. Conf. Med. Image Comput. Comput.-Assist. Intervent*, 2008, pp. 267–275.

[16] H. Amoroso, "Automatic detection of anatomical landmarks in MR brain images," *Int. J. Comput. Assist. Radiol. Surg.*, vol. 5, no. 2, pp. 151–160, 2010.

[17] S. Pereira, F. Rodrigues, and C. Ferreira, "Automatic landmark detection for magnetic resonance imaging based on salient features and discrete deformable models," *Comput. Methods Programs Biomed.*, vol. 111, no. 1, pp. 59–69, 2013.

[18] B. Billot, P. J. Durka, and T. H. Gassert, "Automatic and robust landmark detection and tracking in magnetic resonance imaging time series," *IEEE Trans. Med. Imag.*, vol. 31, no. 2, pp. 235–246, Jun. 2012.

[19] H. Chang, "Automated detection of anatomical landmarks in magnetic resonance images," in *Proc. Int. Conf. Med. Image Comput. Comput.-Assist. Intervent*, 2007, pp. 442–450.

[20] S. K. Lin, R. C. Lo, and R. G. Lee, "MEG–MRI CO-registration using 3D generalized Hough transform," *Biomed. Eng., Appl., Basis Commun.*, vol. 32, no. 4, 2020, Art. no. 2050028, doi: 10.4015/S1016237220500283.

[21] P. Prabhu, "A novel approach to detect anatomical landmarks using R-CNN for MEG-MRI registration," Tech. Rep., Jun. 2022. [Online]. Available: https://ssrn.com/abstract=4139903, doi: 10.2139/ssrn.4139903.

[22] L. Zheng, P. Liao, X. Wu, M. Cao, W. Cui, L. Lu, H. Xu, L. Zhu, B. Lyu, X. Wang, P. Teng, J. Wang, S. Vogrin, C. Plummer, G. Luan, and J.-H. Gao, "An artificial intelligence–based pipeline for automated detection and localisation of epileptic sources from magnetoencephalography," *J. Neural Eng.*, vol. 20, no. 4, Aug. 2023, Art. no. 046036, doi: 10.1088/1741-2552/acef92.

[23] Á. Nárai, "Movement-related artefacts (MR-ART) dataset," [Dataset], *OpenNeuro, Sci. Data* vol 9, no. 1, p. 630. Oct. 2022, doi: 10.18112/openneuro.ds004173.v1.0.2.

[24] R. N. Spreng et al., "Neurocognitive aging data release with behavioral, structural, and multi-echo functional MRI measures," [Dataset], *OpenNeuro, Sci. Data*, vol 9, no. 1, p. 119. Jun. 2022, doi: 10.18112/openneuro.ds003592.v1.0.13.

[25] D. Grssinger, "The role of superstition of cognitive control during neurofeedback training—Part 1," [Dataset], *OpenNeuro, bioRxiv*, Sep. 2023, doi: 10.18112/openneuro.ds004556.v1.0.1.

[26] D. Kingma and J. Ba, "Adam: A method for stochastic optimization," Nov. 2014, *arXiv:1412.6980*.

[27] T. Tieleman and G. Hinton, "Lecture 6.5-RmsProp: Divide the gradient by a running average of its recent magnitude," *COURSERA, Neural Netw. Mach. Learn.*, vol. 4, no. 2, p. 26, 2012.

[28] S. Ruder, "An overview of gradient descent optimization algorithms," 2016, *arXiv:1609.04747*.

[29] J. B. Ludlow, M. Gubler, L. Cevidanes, and A. Mol, "Precision of cephalometric landmark identification: Cone-beam computed tomography vs conventional cephalometric views," *Amer. J. Orthodontics Dentofacial Orthopedics*, vol. 136, no. 3, pp. 312.e1–312.e10, Sep. 2009, doi: 10.1016/j.ajodo.2008.12.018.

M. V. SUHAS received the B.Tech. degree in electronics and communication engineering from Visveswaraya Technological University, Belgaum, Karnataka, India, in 2009, and the M.Tech. degree in digital electronics and advanced communication from Manipal Academy of Higher Education, Manipal, India, in 2011, where he is currently pursuing the Ph.D. degree in biomedical signal processing and analysis. Since 2011, he has been an Assistant Professor with Manipal Institute of Technology, Manipal. His research interests include medical image processing, biomedical signal analysis, and dynamic brain connectivity analysis using MEG. He is a member of IEI.

SANJIB SINHA is currently a Professor with the Department of Neurology, prestigious National Institute of Mental Health and NeuroSciences (NIMHANS), South India, Bengaluru, India. He leads the ''Comprehensive Epilepsy Program'' with NIMHANS, one of the major referral centre for patients with neuropsychiatric illness in India. His research interests include epilepsy, MEG/EEG, sleep, and Wilson's disease and have undertaken several research projects funded by national and international granting agencies. ''Scientific publication'' is his passion, which has resulted in more than 300 peer-reviewed articles, with citations of over 9000. Establishing the MEG facility at NIMHANS, the first of its kind in India, is one of his significant achievements. He is also actively involved in the social and community activities of Indian epilepsy association. He has been involved in training of more than 150 neurologists and nine epileptologists. He has supervised 40 DM/MCh and 12 Ph.D. students for their dissertation work.

N. MARIYAPPA received the Ph.D. degree in physical sciences from HBNI, Mumbai, and the M.Sc. degree in physics from Bharathidasan University, Trichy. Currently, he is a Senior Scientific Officer with the MEG Research Centre, NIMHANS, Bengaluru. His research interests include biomedical signal processing and inverse problem, with a particular emphasis to MCG and MEG signals.

H. ANITHA received the Bachelor of Engineering degree in electronics and communication engineering from Kuvempu University, in 2001, the Master of Technology degree in computer science and engineering from Manipal University, in 2005, and the Ph.D. degree from the Department of Biomedical Engineering, Manipal University, in 2012. She is currently a Professor with the Department of Electronics and Communication Engineering, Manipal Institute of Technology, Manipal, and has over 18 years of experience. Her research interests include biomedical signal and medical image processing and medical image registration. She has been awarded six research grants from bodies, such as DST and ICMR.

KARUNAKAR A. KOTEGAR received the master's degree in computer application from Karnatak University, Dharwad, in 1997, and the Ph.D. degree from MAHE, Manipal, in 2009. He is currently a Professor with the Department of Data Science and Computer Applications, Manipal Institute of Technology (MIT), Manipal. He was a recipient of Fulbright USA and DAAD Germany Fellowships. He was a Postdoctoral Fellow with the Athlone Institute of Technology, Ireland, from June 2010 to November 2011. He is specialized in image and video processing and has to his credit over 50 publications in various national and international journals. One of his research projects was granted U.S. and Indian patents. He has received several awards for poster and paper presentations in national and international fora. He has received The Intellectual Ventures Invention Award, in 2013. He has travelled to more than 28 different nations for various academic, research, and fellowship activities. A vivid speaker, he has conducted around 30 five sessions on NEP-2020 in various forums.